A streamlined protocol and analysis pipeline for CUT&RUN chromatin profiling

Michael P. Meers[1], Terri Bryson[1,2] & Steven Henikoff[1,2*]

[1]Basic Sciences Division, Fred Hutchinson Cancer Research Center, 1100 N. Fairview Ave, Seattle, WA, 98109

[2]Howard Hughes Medical Institute, USA

[*]Corresponding author

Abstract

We previously described a novel alternative to Chromatin Immunoprecipitation, Cleavage Under Targets & Release Using Nuclease (CUT&RUN), in which unfixed permeabilized cells are incubated with antibody, followed by binding of a Protein A-Micrococcal Nuclease (pA/MNase) fusion protein (1). Upon activation of tethered MNase, the bound complex is excised and released into the supernatant for DNA extraction and sequencing. Here we introduce four enhancements to CUT&RUN: 1) a hybrid Protein A-Protein G-MNase construct that expands antibody compatibility and simplifies purification; 2) a modified digestion protocol that prevents premature release of the nuclease-bound complex; 3) a calibration strategy based on carry-over of *E. coli* DNA introduced with the fusion protein; and 4) a novel peak-calling strategy customized for the low-background profiles obtained using CUT&RUN. These new features, coupled with the previously described low-cost, high efficiency, high reproducibility and high-throughput capability of CUT&RUN make it the method of choice for routine epigenomic profiling.

Introduction

Profiling the chromatin landscape for specific components is one of the most widely used methods in biology, and over the past decade, chromatin immunoprecipitation (ChIP) followed by sequencing (ChIP-seq) has become practically synonymous with chromatin profiling (2, 3). However, the most widely used ChIP-seq protocols have limitations and are subject to artifacts (4-7), of which only some have been addressed by methodological improvements (8-12). An inherent limitation to ChIP is that solubilization of chromatin, whether by sonication or enzymatic digestion, results in sampling from the entire solubilized genome, and this requires very deep sequencing so that the sites of targeted protein binding can be resolved above background (2). To overcome this limitation, we introduced Cleavage Under Targets and Release Using Nuclease (CUT&RUN) (1), which is based on the chromatin immunocleavage (ChIC) targeted nuclease strategy (13): Successive incubation of unfixed cells or nuclei with an antibody and a Protein A-Micrococcal Nuclease (pA/MNase) fusion protein is followed by activation of MNase with calcium. In CUT&RUN, cells or nuclei remain intact throughout the procedure and only the targeted sites of binding are released into solution. Our CUT&RUN method dramatically reduced non-specific backgrounds, such that ~10-fold lower sequencing depth was required to obtain similar peak-calling performance (1). In addition, CUT&RUN provides near base-pair resolution, and our most recently published benchtop protocol is capable of profiling ~100 human cells for an abundant histone modification and ~1000 cells for a transcription factor (14). The simplicity of CUT&RUN has also resulted in a fully automated robotic version (AutoCUT&RUN) in which the high reproducibility and low cost makes it ideally suited for high-throughput epigenomic profiling of clinical samples (15). Other advances based on our original CUT&RUN publication include CUT&RUN.Salt for fractionation of chromatin based on solubility (16) and CUT&RUN.ChIP for profiling specific protein components within complexes released by CUT&RUN digestion (17). CUT&RUN has also been adopted by others (18-30), and since publication of our *eLife* paper we have distributed materials to >500 laboratories world-wide, with user questions and answers fielded interactively on our open-access Protocols.io site (31).

Broad implementation of CUT&RUN requires reagent and bioinformatics standardization, and the rapid adoption of CUT&RUN by the larger community of researchers motivates the enhancements described here. First, the method requires a fusion protein that is not at this writing commercially available, and the published pA/MNase purification protocol is cumbersome, which effectively restricts dissemination of the method. Therefore we have produced an improved construct with a 6-His-Tag that can be easily purified using a commercial kit, and by using a Protein A-Protein G hybrid, the fusion protein binds avidly to mouse antibodies, which bind only weakly to Protein A. Second, the original protocols are sensitive to digestion time, in that under-digestion results in low yield and over-digestion can result in premature release of pA/MNase-bound complexes that can digest accessible DNA sites. To address this limitation, we have modified the protocol such that premature release does not occur, allowing digestion to near-completion for high yields with lower backgrounds. Third, the current CUT&RUN protocol recommends a spike-in of heterologous DNA at the release step to compare samples in a series. Here we demonstrate that adding a spike-in is unnecessary, because the carry-over of *E. coli* DNA from purification of pA/MNase or pAG/MNase is sufficient to calibrate samples in a series. Finally, popular peak-calling algorithms designed for ChIP-seq data are crippled by the reduced background noise in CUT&RUN experiments, so we introduce a novel peak-caller that takes advantage of sparse background to define peaks and set thresholds, and we show that it provides better performance on CUT&RUN data than two widely used peak-calling algorithms on both narrow peaks and broad domains.

Results and Discussion

An improved CUT&RUN vector

The pA/MNase fusion protein produced by the pK19-pA-MN plasmid (13) requires purification from lysates of *Escherichia coli* overexpressing cells using an immunoglobulin G (IgG) column, and elution with low pH followed by neutralization has resulted in variations between batches. To improve the purification protocol, we added a 6-His tag (32) into the pK19-pA-MN fusion protein (Figure 1A and Figure 1 – figure supplement 1A). This allowed for simple and gentle purification on a nickel resin column (Figure 1 – figure supplement 1B). In addition, we found

that a commercial 6-His-cobalt resin kit also yielded pure highly active enzyme from a 20 ml culture, enough for ~10,000 reactions. Even when used in excess, there is no increase in release of background fragments (Figure 1 – figure supplement 2), which indicates that the washes are effective in removing unbound fusion protein.

In principle an epitope tagged pAG/MNase could be used for chromatin pull-down from a CUT&RUN supernatant in sequential strategies like CUT&RUN.ChIP (17). However, in practice use of the 6-His tag is complicated by the requirement for a chelating agent to release the protein from the nickel resin. Therefore, we also added an HA (hemagglutinin) tag, which could be used to affinity-purify the complex of a directly bound chromatin particle with a primary antibody and the fusion protein.

Protein A binds well to rabbit, goat, donkey and guinea pig IgG antibodies, but poorly to mouse IgG1, and so for most mouse antibodies, Protein G is generally used (33). To further improve the versatility of the MNase fusion protein, we encoded a single Protein G domain adjacent to the Protein A domain in the pK19-pA-MN plasmid (34). In addition, we mutated three residues in the Protein G coding sequence to further increase binding for rabbit antibodies (35). This resulted in a fusion protein that binds strongly to most commercial antibodies without requiring a secondary antibody. We found that for ordinary CUT&RUN applications pAG/MNase behaves very similarly to pA/MNase, but is more easily purified and is more versatile, for example allowing us to perform CUT&RUN without requiring a secondary antibody for mouse primary monoclonal antibodies (Figure 1B).

Preventing premature release during CUT&RUN digestion

When fragments are released by cleavage in the presence of Ca^{++} ions, the associated pA/MNase complex can diffuse within the nucleus before exiting into the supernatant, resulting in artifactual cleavage of accessible DNA (1). Although performing digestion at 0°C minimizes diffusion, eliminating diffusion during digestion would allow for longer digestion times and more complete release of targeted fragments. Based on the observation that nucleosome core

particles aggregate in high-divalent-cation and low-salt conditions (36), we wondered whether these conditions would prevent diffusion of chromatin particles *in situ*. Therefore, we performed digestions in 10 mM $CaCl_2$ and 3.5 mM HEPES pH 7.5. Under these high-calcium/low-salt conditions, chromatin is digested with no detectable release of fragments into the supernatant (Figure 2A). Reactions are halted by transferring the tube to a magnet, removing the liquid, and adding elution buffer containing 150 mM NaCl, 20 mM EGTA and 25 µg/ml RNAse A, which releases the small DNA fragments into the supernatant. These conditions are compatible with direct end-polishing and ligation used for AutoCUT&RUN (15). Furthermore, retention of the cleaved fragments within the nucleus under high-divalent cation/low-salt conditions could facilitate single-cell application of CUT&RUN.

We usually obtained similar results using either the standard or the high-calcium/low-salt protocol (Figure 2 – figure supplement 1A). However some libraries produced using this modified protocol showed improved consistency of active histone modification peaks when digested over a time-course (Figure 2 – figure supplement 1B), presumably because preventing release of particles during digestion avoids their diffusion within the nucleus where they would artifactually digest accessible DNA. The close correlations between high-calcium/low-salt H3K27ac datasets for time points over a ~30-fold range (Figure 2B) occur with corresponding increases in the yield of fragments released into the supernatant during subsequent elution (Figure 2 – figure supplement 2). We observed similarly high signal-to-noise levels for the CTCF sequence-specific DNA-binding protein over the same time-course using both pA/MNase and pAG/MNase (Figure 2C). This indicates that longer digestion times result in higher yields, with high signal-to-noise throughout the digestion series (Figure 2D). Thus, this modification of CUT&RUN can reduce the risk of overdigestion.

We previously showed that CUT&RUN can be performed on insoluble protein complexes by extracting total DNA (1) or by performing salt fractionation of the bead-bound cells and extracting DNA from the residual pellet (16). In either case, large DNA fragments were depleted using SPRI (AMPure XP) beads before library preparation. We confirmed that this total DNA

extraction protocol gives similar results for both standard and high-calcium/low-salt digestion (Figure 2 – figure supplement 1A). RNA polymerase II (RNAPII) from animal cells is also insoluble when engaged (37, 38), and requires harsh treatments for quantitative profiling using ChIP (39). To determine whether our high-calcium/low-salt CUT&RUN protocol can be used for insoluble chromatin complexes, we profiled Serine-5-phosphate on the C-terminal domain (CTD) of the Rpb1 subunit of RNAPII using both salt fractionation and total DNA extraction. This CTD phosphorylation is found in the initiating form of RNAPII, and we observed similar genic 5'-end-enriched profiles for soluble, insoluble and total DNA (Figure 1B). Although we observed similarly low background levels over a 10-fold digestion range using the standard or the high-calcium/low-salt protocol, backgrounds were relatively high using the standard protocol digestion for both rabbit and mouse antibodies (Figure 1B, compare 30 min digestions). This example suggests that preventing release with the modified protocol can improve CUT&RUN data quality during extended digestions.

Calibration using *E. coli* carry-over DNA

Comparing samples in a series typically requires calibration for experimental quality and sequencing read depth. It is common to use background levels to calibrate ChIP-seq samples in a series and to define and compare peaks for peak-calling (2). However, the extremely low backgrounds of CUT&RUN led us to a calibration strategy based on spike-in of heterologous DNA, which has been generally recommended for all situations in which samples in a series are to be compared (40, 41). In our current spike-in protocol, the heterologous DNA, which is typically DNA purified from an MNase digest of yeast *Saccharomyces cerevisiae* or *Drosophila melanogaster* chromatin, is added when stopping a reaction, and we adopted this spike-in procedure for the high-calcium/low-salt protocol described in the previous section. Interestingly, we noticed that mapping reads to both the spike-in genome and the *E. coli* genome resulted in almost perfect correlation (R^2=0.97) between *S. cerevisiae* and *E. coli* in an experiment using pA/MNase in which the number of cells was varied over several orders of magnitude (Figure 3A). Near-perfect correlations (R^2=0.96-0.99) between yeast spike-in and carry-over *E. coli* DNA were also seen in series using pAG/MNase with high-calcium/low-salt

digestion conditions (Figure 3B), and for both supernatant release and extraction and total DNA extraction (Figure 3C-D). These strong positive correlations are not accounted for by cross-mapping of the yeast spike-in to the *E. coli* genome, because omitting the spike-in for a low-abundance epitope resulted in very few yeast counts with high levels of *E. coli* counts (blue symbol in Figure 3C-D panels). As the source of *E. coli* DNA is carried over from purification of pA/MNase and pAG/MNase, the close correspondence provides confirmation of the accuracy of our heterologous spike-in procedure (1). Moreover, as carry-over *E. coli* DNA is introduced at an earlier step, and is cleaved to small mappable fragments that are released during digestion and elution, it provides a more desirable calibration standard than using heterologous DNA (40, 41). High correlations were also seen between *S. cerevisiae* spike-in and *E. coli* carry-over DNA for pA-MNase in batches that we have distributed (Figure 3 – table supplement 1). Therefore, data for nearly all CUT&RUN experiments performed thus far can be recalibrated *post-hoc* whether or not a spike-in calibration standard had been added.

Peak-calling based on fragment block aggregation

Peak calling algorithms designed for the analysis of ChIP-seq data are often optimized for high recall to distinguish signal from background (42). However, the low read depths of CUT&RUN data render standard peak callers vulnerable to reduced precision (i.e. avoidance of false positives) due to the sparseness of the background, resulting in any spurious background read being called as a peak. To address this problem we developed Sparse Enrichment Analysis for CUT&RUN (SEACR), a peak-calling algorithm that enforces precision from sparse data by quantifying the global distribution of background signal and using it to set a stringent empirical threshold for peak identity. CUT&RUN data from target antibody and IgG control experiments are first parsed into “signal blocks” representing segments of continuous, non-zero read depth, and the signal in each block is calculated by summing read counts (Figure 4A). A plot of the proportion of signal blocks in Target or IgG (y-axis) is used to identify the threshold value at which the percentage of Target versus IgG blocks is maximized; then target blocks failing to meet the threshold are filtered out, leaving enriched “peaks” (Figure 4A). We also filtered out

blocks that overlap an IgG block meeting the threshold as a means to eliminate spurious peaks that arise either through multiple mapping at repeated regions or by "hyper-accessibility" (4).

To test the performance of SEACR in comparison with popular peak calling algorithms designed for ChIP-seq, we used SEACR, MACS2 and HOMER to call peaks from CUT&RUN data for two transcription factors (TFs), Sox2 and FoxA2 in human embryonic stem cells (hESCs) and Definitive Endoderm (DE) cells. Sox2 expression is restricted to hESCs and FoxA2 expression is restricted to DE cells. SEACR succeeded in calling a comparable number of peaks for Sox2 in hESCs or FoxA2 in DE cells as either MACS2 (43) or HOMER (44), while calling only 1-4 peaks for either factor when they are not expressed (Figure 4B, "AUC only"). In contrast, both HOMER and MACS2 called up to ~900 spurious peaks in these datasets; these trends held when analyzing total bases covered by peaks or percentage of reads in peaks (Figure 4—figure supplement 1A-B). We also sought to increase the recall (i.e. detection of true positives) of SEACR by including peaks that meet a maximum signal threshold (i.e. the highest read depth in the signal block) that may not have met the total signal threshold described above. We found that this approach yielded more peaks with nearly identical precision (Figure 4B, Figure 4—figure supplement 1A-B, "union").

To test SEACR performance across a spectrum of read depths, we called peaks using SEACR union mode (owing to its improved recall and comparable precision), MACS2, and HOMER, from H3K4me2 CUT&RUN data subsampled 10 times each at 11 different read depths spanning from 2M to 40M reads. When called peaks were compared with a stringent test set of peaks (-log10 FDR > 10) called by the ENCODE consortium using MACS2 on ENCODE ChIP-seq data, SEACR consistently minimized the fraction of called peaks that were outside the test set. This indicates that the precision of SEACR is robust across a range of read depths (Figure 5A-C). Precision at 30M and 40M reads were notable exceptions, which likely owes to the total signal threshold becoming less stringent by the lack of sparse background. SEACR maintained higher recall than HOMER across most read subsampling levels, as measured by the percentage of test set peaks overlapping CUT&RUN peaks called by the algorithm; however, in several cases recall

was less than that of MACS2 at the same read depth level. To analyze the general optimality of combined recall and precision for each peak caller, we calculated the F1 score for each peak caller at each read subsampling level, such that larger F1 scores corresponded with higher performance in a combination of the two metrics. SEACR exhibited superior performance at all subsampling levels between 5M and 25M reads (Figure 5D). Although our conclusions are based on the presumption that high-scoring ENCODE peaks are true positives, the fact that they were called using MACS2 leads us to expect that the superior performance of SEACR on CUT&RUN data will generalize to any set of presumed true positives. Thus, SEACR is an optimal peak caller for CUT&RUN data across a range of read depths, and maintains a high percentage of true positive peak calls at low read depth.

Uniform peak calling is often confounded by the diverse distributions of chromatin proteins and modifications; for instance, transcription factors are expected to cluster at narrow genomic loci and adopt a typical "peaked" data structure, whereas many histone modifications such as H3K27me3 cover broad regions that are not easily summarized by the same methods that detect typical peaks. Since our signal block approach is agnostic to region width, we reasoned that SEACR might be equally successful at identifying broad domains as the peaks identified from Sox2, FoxA2, and H3K4me2 data. To test this, we called peaks using SEACR, MACS2 and HOMER (using "broad" or "histone" settings for the latter two) from an H3K27me3 CUT&RUN dataset (15) that contains broad domains by visual inspection. Remarkably, though SEACR called many fewer enriched regions than MACS2 or HOMER (28803, 97247, and 104524, respectively), SEACR regions covered more sequence (31.4 Mb) than either (28.1Mb and 18.3 Mb), indicating that SEACR regions are broader. Indeed, the average width of SEACR regions exceeded that of MACS2 and HOMER by nearly an order of magnitude (Figure 6A). Visual inspection of loci with broad H3K27me3 domains such as the HOXD cluster indicates that, whereas MACS2 and HOMER partition the domain into several subregions, SEACR maintains the majority of the domain structure in a limited number of large signal blocks (Figure 6B). These data indicate that SEACR is a promising tool for identifying large domains in CUT&RUN data in addition to spatially restricted binding sites.

Conclusions

Since its introduction in our original *eLife* paper (1), the advantages of CUT&RUN over ChIP-seq has led to its rapid adoption, including publication of new CUT&RUN protocols for low cell numbers (14, 23), for plant tissues (25) and for high-throughput (15). The new CUT&RUN advances that we describe here are likely to be useful when applied in all of these protocols. Our improved CUT&RUN fusion construct simplifies reagent purification and eliminates the requirement for a secondary antibody against mouse primary antibodies. Our high-calcium/low-salt protocol minimizes time-dependent variability. Our discovery that carry-over *E. coli* DNA almost perfectly correlates with an added spike-in upgrades a contaminant to a resource that can be used as a spike-in calibration proxy, even *post-hoc* simply by counting reads mapping to the *E. coli* genome in existing CUT&RUN datasets.

We have also introduced a novel peak-calling strategy that takes advantage of the precise position and fragment spanning information that is present in CUT&RUN data. Popular peak-calling programs were designed around ChIP-seq data, where fragment spans are lacking owing to the widespread use of sonication and single-end sequencing. In contrast, our SEACR algorithm finds peaks in CUT&RUN data with a better precision/recall trade-off than the most popular ChIP-inspired peak-callers. SEACR is also likely to be useful for other epigenomic datasets that capture fragment position and length information with high signal-to-noise. We expect that as the value of precise fragment information becomes better appreciated, for example in inferring chromatin dynamics (45), our block aggregation strategy will become increasingly powerful.

Materials and methods

Cell culture

K562 cells and H1 hESCs were cultured as previously described (15). Definitive endoderm (DE) was derived from a culture of H1 hESCs using the StemDiff Definitive Endoderm kit (StemCell Technologies).

Construction and purification of an improved IgG-affinity/MNase fusion protein

Hemagglutinin and 6-histidine tags were added to the carboxyl-terminus of pA-MNase (13) using a commercially synthesized dsDNA fragment (gBlock®) from Integrated DNA Technologies (IDT), which contains the coding sequence for both tags, glycine-rich flexible linkers and includes restriction sites for cloning. Another IDT gBlock® containing the optimized protein-G coding sequence and homologous flanking regions to the site of insertion, was introduced via PCR overlap extension using Gibson Assembly® Master Mix (New England Biolabs cat. #E2611), following the manufacturer's instructions. The sequence-verified construct was transformed into JM101 cells (Agilent Technologies cat. #200234) for expression, cultured in NZCYM-Kanamycin (50 µg/ml) and induced with 2 mM Isopropyl β-D-1-thiogalactopyranoside following standard protein expression and purification protocols. The cell pellet was resuspended in 10 ml Lysis Buffer, consisting of 10mM Tris-HCL pH 7.5, 300mM NaCl, 10mM Imidazole, 5mM beta-mercaptoethanol, and EDTA-free protease inhibitor tablets at the recommended concentration (Sigma-Aldrich cat. #5056489001). Lysis using chicken egg white lysozyme (10 mg/mL solution, EMD cat. #71412 solution) was followed by sonication with a Branson Sonifier blunt-end adapter at output level 4, 45 seconds intervals for 5-10 rounds or until turbidity was reduced. The lysate was cleared by high-speed centrifugation and purified over a nickel-agarose column, taking advantage of the poly-histidine tag for efficient purification via immobilized metal affinity chromatography. Cleared lysate was applied to a 20 ml disposable gravity-flow column 1.5 ml (0.75 ml bed volume) of NI-NTA agarose (Qiagen cat. #30210), washed twice in three bed volumes of Lysis Buffer. Lysate was applied followed by two washes at five bed volumes of 10 mM Tris-HCl pH 7.5, 300 mM NaCl, 20 mM Imidazole, 0.03% ZWITTERGENT 3-10 Detergent (EMD Millipore cat. #693021) and EDTA-free protease inhibitor tablets. Elution was performed with 1 ml 10 mM Tris-HCl pH 7.5, 300 mM NaCl, 250 mM Imidazole and EDTA-free protease inhibitor tablets. Eluate was dialyzed twice against a 750 ml volume of 10mM Tris-HCl pH 7.5 , 150 mM NaCl, 1 mM EDTA, 1 mM PMSF to remove imidazole. Glycerol was then added to 50%, aliquots stored at –80 ^{o}C for long term storage and –20 ^{o}C for working stocks.

For purification, we used either the nickel-based protocol or the Pierce Cobalt kit (Pull-Down PolyHis Protein:Protein Interaction Kit cat. #21277 from Thermo Fisher). Similar results were obtained using either the nickel or cobalt protocol, although the cobalt kit alleviated the need for a sonicator, using a fifth of the starting material from either fresh culture or a cell pellet frozen in lysis buffer, and yielded more protein per volume of starting material. With the cobalt kit, 20 ml of culture yielded ~100 µg of fusion protein.

CUT&RUN using high-calcium/low-salt digestion conditions

Log-phase cultures of K562 cells were harvested, washed, and bound to activated Concanavalin A-coated magnetic beads, then permeabilized with Wash buffer (20 mM HEPES, pH7.5, 150 mM NaCl, 0.5 mM spermidine and a Roche complete tablet per 50 ml) containing 0.05% Digitonin (Dig-Wash) as described (14). The bead-cell slurry was incubated with antibody in a 50-100 µL volume for 2 hr at room temperature or at 4°C overnight on a nutator or rotator essentially as described (14). In some experiments, cells were permeabilized and antibody was added and incubated 2 hr to 3 days prior to addition of ConA beads with gentle vortexing; similar results were obtained (*e.g.* Figure 2B-D), although with lower yields. After 2-3 washes in 1 ml Dig-wash, beads were resuspended in 50-100 µL pA/MNase or pAG/MNase and incubated for 1 hr at room temperature. After 2 washes in Dig-wash, beads were resuspended in low-salt rinse buffer (20 mM HEPES, pH7.5, 0.5 mM spermidine, a Roche mini-complete tablet per 10 ml and 0.05% Digitonin). Tubes were chilled to 0°C, the liquid was removed on a magnet stand, and ice-cold calcium incubation buffer (Dig-wash containing 10 mM $CaCl_2$) was added while gently vortexing. Tubes were replaced on ice during the incubation for times indicated in each experiment, and within 30 seconds of the end of the incubation period the tubes were replaced on the magnet, and upon clearing, the liquid was removed, followed by immediate addition of EGTA-STOP buffer (170 mM NaCl, 20 mM EGTA, 0.05% Digitonin, 20 µg/ml glycogen, 25 µg/ml RNase A, 2 pg/ml *S. cerevisiae* fragmented nucleosomal DNA). Beads were incubated at 37°C for 30 min, replaced on a magnet stand and the liquid was removed to a fresh tube and DNA was extracted as described (14). A detailed step-by-step protocol is available at

https://www.protocols.io/view/cut-run-targeted-in-situ-genome-wide-profiling-wit-n6wdhfe/abstract. Extraction of pellet and total DNA was performed essentially as described (1, 16).

DNA sequencing and data processing. The size distribution of libraries was determined by Agilent 4200 TapeStation analysis, and libraries were mixed to achieve equal representation as desired aiming for a final concentration as recommended by the manufacturer. Paired-end Illumina sequencing was performed on the barcoded libraries following the manufacturer's instructions. Paired-end reads were aligned using Bowtie2 version 2.2.5 with options: --local --very-sensitive-local --no-unal --no-mixed --no-discordant --phred33 -I 10 -X 700. For MACS2 peak calling, parameters used were macs2 callpeak – t input_file –p 1e-5 –f BEDPE/BED(Paired End vs. Single End sequencing data) –keep-dup all –n out_name. Some datasets showed contamination by sequences of undetermined origin consisting of the sequence $(TA)_n$. To avoid cross-mapping, we searched blastn for TATATATATATATATATATATATAT against hg19, collapsed the overlapping hits into 34,832 regions and intersected with sequencing datasets, keeping only the fragments that did not overlap any of these regions.

Evaluating time-course data

If digestion and fragment release into the supernatant occur linearly with time of digestion until all fragments within a population are released, then we expect that CUT&RUN features will be linearly correlated within a time-course series. For CTCF, features were significant CTCF motifs intersecting with DNAseI hypersensitive sites (1). For H3K27Ac and H3K4me2, we called peaks using MACS2 and calculated the Pearson correlation coefficients between time points, displayed as a matrix of R^2 values, using the following procedure:

1) Aligned fastq files to unmasked genomic sequence using Bowtie2 version 2.2.5 to UCSC hg19 with parameters: --end-to-end --very-sensitive --no-mixed --no-discordant -q --phred33 -I 10 -X 700.

2) Extracted properly paired read fragments from the alignments and pooled fragments from multiple samples.

3) Compared pooled fragments with $(TA)_n$ regions of hg19 and kept those fragments that did NOT overlap any $(TA)_n$ region using bedtools 2.21.0 with parameters: intersect -v -a fragments.bed -b TATA_regions.bed > fragments_not_TATA.bed.

4) Found peaks using macs2 2.1.1.20160309 with parameters: callpeak -t fragments_not_mask.bed -f BED -g hs --keep-dup all -p 1e-5 -n not_mask –SPMR.

5) Made scaled fractional count bedgraph files for each sample from bed files made in step 2. The value at each base pair is the fraction of counts times the size of hg19 so if the counts were uniformly distributed the value would be 1 at each bp.

6) Extracted bedgraph values for ±150 bps around peak summits for IgG sample and computed their means, which resulted in one mean score per peak.

7) Removed peaks from macs2 results in step 4 if the mean score was greater than the 99th percentile of all IgG scores to make a subset of the peaks lacking the most extreme outliers.

8) Extracted bedgraph values for ±150 bps around the subset of peak summits from step 7 for all samples and computed their means, which resulted in a matrix with columns corresponding to samples and one row per peak.

9) Computed correlations of matrix in 8 using R 3.2.2 cor(matrix, use="complete.obs") command.

SEACR: Sparse Enrichment Analysis for CUT&RUN

SEACR was designed to call enriched regions from sparse CUT&RUN data, in which background is dominated by “zeroes” (i.e. regions with no read coverage). SEACR takes as input the following four fields: 1) Target data bedgraph file in UCSC bedgraph format (https://genome.ucsc.edu/goldenpath/help/bedgraph.html) that omits regions containing 0 signal; 2) Control (IgG) data bedgraph file; 3) “norm” denotes normalization of control to target data, “non” skips this behavior; 4) “union” forces implementation of a maximum signal threshold in addition to the total signal threshold, and corresponds to the “union” mode described in the text, whereas “AUC” avoids this behavior, and corresponds to “AUC only” mode.

Briefly, for each input bedgraph, we concatenated each region with adjacent regions to generate "signal blocks" that span all concatenated component regions, and calculated total signal for each signal block by taking the sum across all component regions of the region length (region end minus region start) multiplied by its bedgraph signal (column 4):

$$t = \sum_{i=1}^{n} (end_i - start_i) * (signal_i)$$

We designated maximum signal for each signal block as the maximum bedgraph signal value for any component region contained in the block. For normalization, we generated total signal density plots for all signal blocks from target and control data, identified the total signal AUC values that corresponded to the density peak of each plot, and multiplied total signal values for all control signal blocks by a "scaling factor" calculated by dividing the density peak total signal value for target data by the density peak total signal value for control data. To determine the total signal threshold *t*, we identified the value corresponding to the maximum value of *F* for the following function:

$$for\ t \in \{0, \cdots, T\};\ F = \frac{\sum_{i=1}^{m}[r_i > 0] - \sum_{i=1}^{m}[r_i > t]}{\sum_{j=1}^{n}[s_j > 0] - \sum_{j=1}^{n}[s_j > t]}$$

Where *T* is the maximum total signal value in any signal block, r_i is the total signal for an element *i* in the set of *m* target signal blocks, s_j is the total signal for an element *j* in the set of *n* target or control signal blocks, and *F* is the fraction of target signal blocks divided by total signal blocks remaining above threshold *t*. Once *t* is established, all target signal blocks exceeding *t* that do not overlap a control signal block that also exceeds *t* are retained. For "union" mode, a similar threshold calculation is implemented for maximum signal, and any target signal blocks exceeding *t* for maximum signal that don't overlap control blocks exceeding *t* for total signal are also retained.

MACS2 peaks were called using macs2 callpeak -f BEDPE --keep-dup all, with treatment and control files. For H3K27me3, the --broad flag was added. HOMER peaks were called by generating tag directories for target and control datasets, then using findPeaks, -style factor for TFs or H3K4me2, and -style histone for H3K27me3. For recall and precision analysis, we used ENCODE H3K4me2 ChIP-seq peaks (ENCFF099LMD) meeting a –log10(FDR) cutoff of 10 as the test set, and used bedtools intersect with the –u flag to calculate the percentage of test set regions overlapped (fraction of true positives) or the percentage of experimental peaks outside the test set (fraction of false positives). F1 scores were calculated as follows:

$$F = \frac{2 * (P * R)}{P + R}$$

Where *P* is precision (fraction of called peaks that are true positives) and *R* is recall (fraction of true positives from test set identified).

Availability

The plasmid pAG-ERH-MNase-6xHIS-HA is available from Addgene. Sequencing datasets are available from GEO (GSE126612). All scripts associated with SEACR are provided at https://github.com/mpmeers/SEACR.

Acknowledgements

We thank Jorja Henikoff for data processing and analysis, and Christine Codomo and Tayler Hentges for technical support. We also thank all members of the Henikoff lab for valuable discussions and Kami Ahmad, Brian Freie and Bob Eisenman for comments on the manuscript. This work was supported by the Howard Hughes Medical Institute, and a grant from the National Institutes of Health (4DN TCPA A093) and the Chan-Zuckerberg Initiative.

Author contributions

M.P.M and S.H. designed and performed all profiling experiments. T.D.B. designed and produced the pAG/MNase fusion construct. M.P.M. developed algorithms and M.P.M. and S.H analyzed the data. M.P.M, T.D.B and S.H. wrote the manuscript.

Competing interests

The authors declare no competing interests.

References

1. Skene PJ, Henikoff S. An efficient targeted nuclease strategy for high-resolution mapping of DNA binding sites. eLife. 2017;6:e21856.

2. Landt SG, Marinov GK, Kundaje A, Kheradpour P, Pauli F, Batzoglou S, et al. ChIP-seq guidelines and practices of the ENCODE and modENCODE consortia. Genome Res. 2012;22(9):1813-31.

3. Schubert C. Technology Feature: ChIP off the old block: Beyond chromatin immunoprecipitation. Science. 2018;362(6419):1190-2.

4. Teytelman L, Thurtle DM, Rine J, van Oudenaarden A. Highly expressed loci are vulnerable to misleading ChIP localization of multiple unrelated proteins. Proc Natl Acad Sci U S A. 2013;110(46):18602-7.

5. Park D, Lee Y, Bhupindersingh G, Iyer VR. Widespread misinterpretable ChIP-seq bias in yeast. PLoS One. 2013;8(12):e83506.

6. Jain D, Baldi S, Zabel A, Straub T, Becker PB. Active promoters give rise to false positive 'Phantom Peaks' in ChIP-seq experiments. Nucleic Acids Res. 2015;43(14):6959-68.

7. Teves SS, An L, Hansen AS, Xie L, Darzacq X, Tjian R. A dynamic mode of mitotic bookmarking by transcription factors. eLife. 2016;5:e22280.

8. Zhang Z, Pugh BF. High-resolution genome-wide mapping of the primary structure of chromatin. Cell. 2011;144(2):175-86.

9. Kasinathan S, Orsi GA, Zentner GE, Ahmad K, Henikoff S. High-resolution mapping of transcription factor binding sites on native chromatin. Nature Methods. 2014;11:203-9.

10. Brind'Amour J, Liu S, Hudson M, Chen C, Karimi MM, Lorincz MC. An ultra-low-input native ChIP-seq protocol for genome-wide profiling of rare cell populations. Nat Commun. 2015;6:6033.

11. Rossi MJ, Lai WKM, Pugh BF. Simplified ChIP-exo assays. Nat Commun. 2018;9(1):2842.

12. van Galen P, Viny AD, Ram O, Ryan RJ, Cotton MJ, Donohue L, et al. A Multiplexed System for Quantitative Comparisons of Chromatin Landscapes. Mol Cell. 2016;61(1):170-80.

13. Schmid M, Durussel T, Laemmli UK. ChIC and ChEC; genomic mapping of chromatin proteins. Mol Cell. 2004;16(1):147-57.

14. Skene PJ, Henikoff JG, Henikoff S. Targeted in situ genome-wide profiling with high efficiency for low cell numbers. Nat Protoc. 2018;13(5):1006-19.

15. Janssens DH, Wu SJ, Sarthy JF, Meers MP, Myers CH, Olson JM, et al. Automated in situ chromatin profiling efficiently resolves cell types and gene regulatory programs. Epigenetics Chromatin. 2018;11(1):74.

16. Thakur J, Henikoff S. Unexpected conformational variations of the human centromeric chromatin complex. Genes Dev. 2018;32(1):20-5.

17. Brahma S, Henikoff S. RSC-Associated Subnucleosomes Define MNase-Sensitive Promoters in Yeast. Mol Cell. 2019;73(2):238-49.

18. Liu N, Hargreaves VV, Zhu Q, Kurland JV, Hong J, Kim W, et al. Direct Promoter Repression by BCL11A Controls the Fetal to Adult Hemoglobin Switch. Cell. 2018;173(2):430-42.

19. Roth TL, Puig-Saus C, Yu R, Shifrut E, Carnevale J, Li PJ, et al. Reprogramming human T cell function and specificity with non-viral genome targeting. Nature. 2018;559(7714):405-9.

20. de Bock CE, Demeyer S, Degryse S, Verbeke D, Sweron B, Gielen O, et al. HOXA9 Cooperates with Activated JAK/STAT Signaling to Drive Leukemia Development. Cancer discovery. 2018;8(5):616-31.

21. Park SM, Cho H, Thornton AM, Barlowe TS, Chou T, Chhangawala S, et al. IKZF2 Drives Leukemia Stem Cell Self-Renewal and Inhibits Myeloid Differentiation. Cell Stem Cell. 2019;24(1):153-65.

22. Inoue A, Chen Z, Yin Q, Zhang Y. Maternal Eed knockout causes loss of H3K27me3 imprinting and random X inactivation in the extraembryonic cells. Genes Dev. 2018;32(23-24):1525-36.

23. Hainer SJ, Fazzio TG. High-Resolution Chromatin Profiling Using CUT&RUN. Current protocols in molecular biology / edited by Frederick M Ausubel [et al]. 2019:e85.

24. Oomen ME, Hansen AS, Liu Y, Darzacq X, Dekker J. CTCF sites display cell cycle-dependent dynamics in factor binding and nucleosome positioning. Genome Res. 2019;29:236-49.

25. Zheng XY, Gehring M. Low-input chromatin profiling in Arabidopsis endosperm using CUT&RUN. Plant reproduction. 2019; https://link.springer.com/article/10.1007/s00497-018-00358-1.

26. Hainer SJ, Boškovic A, Rando OJ, Fazzio TG. Profiling of pluripotency factors in individual stem cells and early embryos. bioRxiv. 2018; https://www.biorxiv.org/content/10.1101/286351v2.

27. Ahmad K, Spens A. Separate Polycomb Response Elements control chromatin state and activation of the vestigial gene. biorxiv. 2018; https://www.biorxiv.org/content/early/2018/12/05/488478.

28. Uyehara CM, McKay DJ. A direct and widespread role for the nuclear receptor EcR in mediating the response to ecdysone in Drosophila. biorxiv. 2019; https://www.biorxiv.org/content/early/2019/01/10/517458.

29. Federation AJ, Nandakumar V, Wang H, Searle B, Pino L, Merrihew G, et al. Quantification of nuclear protein dynamics reveals chromatin remodeling during acute protein degradation. biorxiv. 2018; https://www.biorxiv.org/content/early/2018/06/30/345686.

30. Daneshvar K, Ardehal MV, Klein IA, Kratkiewicz AJ, Zhou C, Mahpour A, et al. lncRNA DIGIT and BRD3 protein form phase-separated condensates to regulate endoderm differentiation. biorxiv. 2019; https://www.biorxiv.org/content/10.1101/547513v1:547513v1.

31. Skene PJ, Henikoff S. CUT&RUN: Targeted in situ genome-wide profiling with high efficiency for low cell numbers. Protocols.io 2018 Available from: 10.17504/protocols.io.mgjc3un.

32. Bornhorst JA, Falke JJ. Purification of proteins using polyhistidine affinity tags. Methods Enzymol. 2000;326:245-54.

33. Fishman JB, Berg EA. Protein A and Protein G Purification of Antibodies. Cold Spring Harbor protocols. 2019;2019(1):pdb prot099143.

34. Eliasson M, Olsson A, Palmcrantz E, Wiberg K, Inganas M, Guss B, et al. Chimeric IgG-binding receptors engineered from staphylococcal protein A and streptococcal protein G. J Biol Chem. 1988;263(9):4323-7.

35. Jha RK, Gaiotto T, Bradbury AR, Strauss CE. An improved Protein G with higher affinity for human/rabbit IgG Fc domains exploiting a computationally designed polar network. Protein engineering, design & selection : PEDS. 2014;27(4):127-34.

36. de Frutos M, Raspaud E, Leforestier A, Livolant F. Aggregation of nucleosomes by divalent cations. Biophys J. 2001;81(2):1127-32.

37. Weber CM, Ramachandran S, Henikoff S. Nucleosomes are context-specific, H2A.Z-modulated barriers to RNA polymerase. Mol Cell. 2014;53(5):819-30.

38. Mayer A, Iulio J, Maleri S, Eser U, Vierstra J, Reynolds A, et al. Native elongating transcript sequencing reveals human transcriptional activity at nucleotide resolution. Cell. 2015;161:541-54.

39. Skene PJ, Henikoff S. A simple method for generating high-resolution maps of genome wide protein binding. eLife. 2015;4:e09225.

40. Chen K, Hu Z, Xia Z, Zhao D, Li W, Tyler JK. The Overlooked Fact: Fundamental Need for Spike-In Control for Virtually All Genome-Wide Analyses. Mol Cell Biol. 2015;36(5):662-7.

41. Hu B, Petela N, Kurze A, Chan KL, Chapard C, Nasmyth K. Biological chromodynamics: a general method for measuring protein occupancy across the genome by calibrating ChIP-seq. Nucleic Acids Res. 2015;43(20):e132.

42. Liu T. Use model-based Analysis of ChIP-Seq (MACS) to analyze short reads generated by sequencing protein-DNA interactions in embryonic stem cells. Methods Mol Biol. 2014;1150:81-95.

43. Zhang Y, Liu T, Meyer CA, Eeckhoute J, Johnson DS, Bernstein BE, et al. Model-based analysis of ChIP-Seq (MACS). Genome Biol. 2008;9(9):R137.

44. Heinz S, Benner C, Spann N, Bertolino E, Lin YC, Laslo P, et al. Simple combinations of lineage-determining transcription factors prime cis-regulatory elements required for macrophage and B cell identities. Mol Cell. 2010;38(4):576-89.

45. Ramachandran S, Ahmad K, Henikoff S. Transcription and Remodeling Produce Asymmetrically Unwrapped Nucleosomal Intermediates. Mol Cell. 2017;68(6):1038-53.

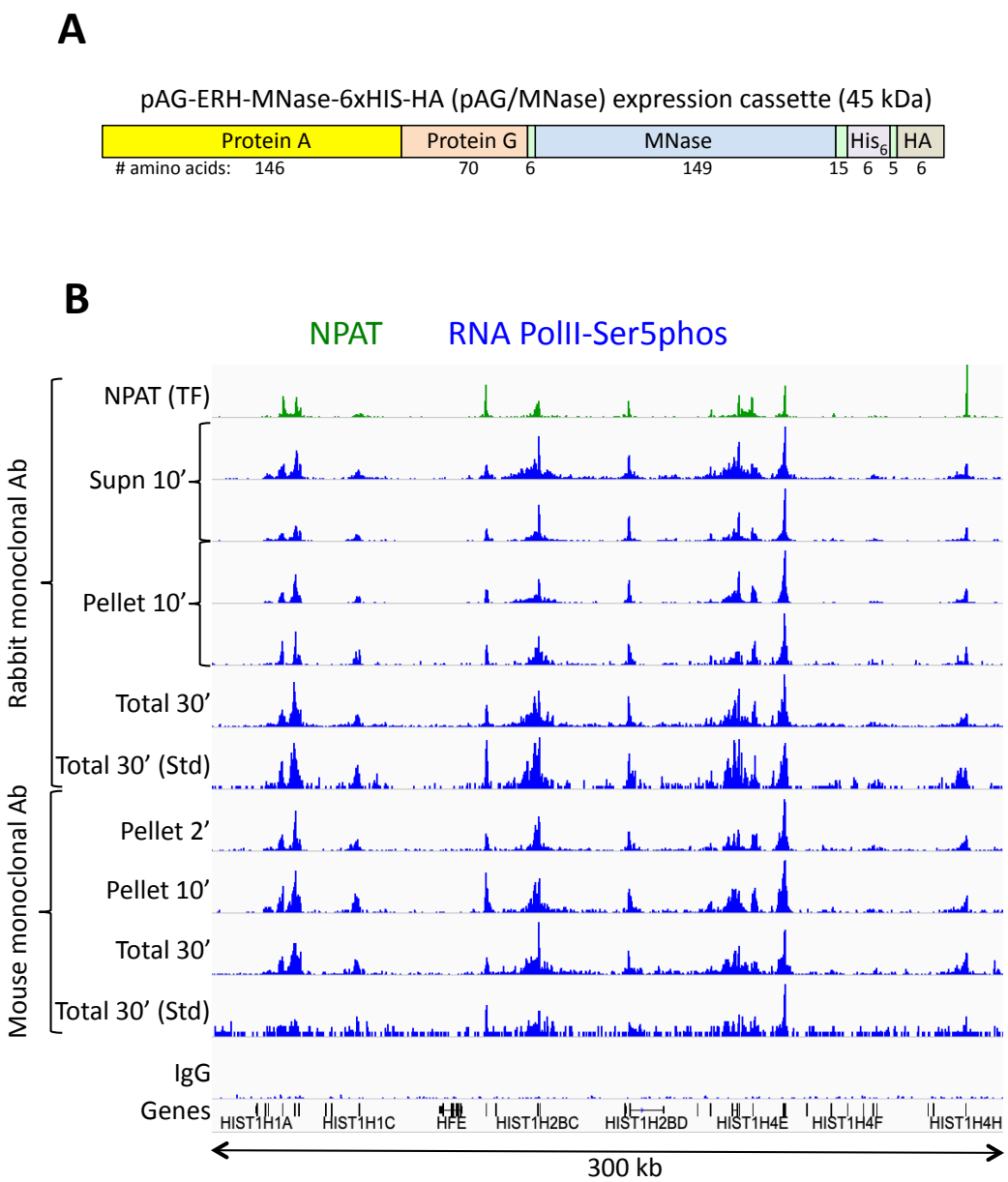

Figure 1. An improved fusion protein for CUT&RUN. A) Schematic diagram (not to scale) showing improvements to the pA-MNase fusion protein, which include addition of the C2 Protein G IgG binding domain, a 6-histidine tag for purification and a hemagglutinin tag (HA) for immunoprecipitation. **B**) The Protein A/G hybrid fusion results in high-efficiency CUT&RUN for both rabbit and mouse primary antibodies. CUT&RUN for both rabbit and mouse RNAPII-Ser5phosphate using pAG/MNase and low-salt/high-calcium conditions shows high signal-to-noise when extracted from the insoluble pellet. Tracks are shown for the histone gene cluster at Chr6:26,000,000-26,300,000, where NPAT is a transcription factor that co-activates histone genes. After digestion in low-salt/high-calcium conditions, both the supernatant and pellet fractions were extracted, resulting in similar profiles for two biological replicates. Extracting all DNA after a 30 min digestion showed high signal-to-noise for high-calcium/low-salt condtions relative to that using the standard protocol performed in parallel. Tracks are autoscaled except for the IgG negative control which was reduced 10-fold.

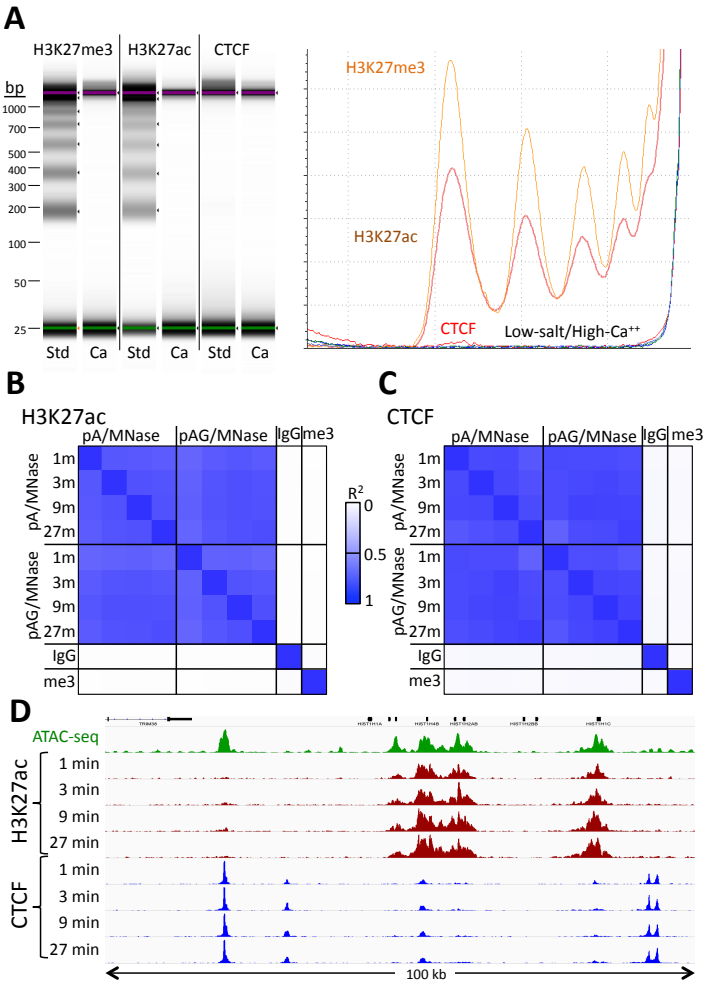

Figure 2. Consistent peak definition with high-Ca++/low salt digestion. A) CUT&RUN was performed using either the high-Ca^{++}/low-salt (Ca^{++}) or the standard (Std) method with antibodies to three different epitopes. DNA was extracted from supernatants, where no elution was carried out for the Ca^{++} samples. Although high yields of nucleosomal ladder DNA eluted from the supernatants using the standard method, no DNA was detectable in the supernatant using the high-Ca^{++}/low salt method when the elution step was omitted. Left, Tapestation images from indicated lanes; Right, Densitometry of the same lanes. **B**) CUT&RUN was performed with an antibody to H3K27ac (Millipore MABE647) and to CTCF (Millipore 07-729) with digestion over a 1 to 27 min range as indicated using pA/G-MNase with the high-Ca^{++}/low-salt protocol. Correlation matrix comparing peak overlap for time points and fusion constructs. The datasets were pooled and MACS2 was used with default parameters to call peaks, excluding those in repeat-masked intervals and those where peaks overlapped with the top 1% of IgG occupancies, for a total of 52,425 peaks. Peak positions were scored for each dataset and correlations (R^2 displayed with Java TreeView v.1.16r2, contrast = 1.25) were calculated between peak vectors. IgG and H3K27me3 (me3) negative controls were similarly scored. **C**) Same as B, except the antibody was to CTCF. A set of 9,403 sites with a CTCF motif within a hypersensitive site was used (1). High correlations between all time points demonstrate the uniformity of digestion over a 27-fold range. **D)** Representative tracks from datasets used for panels B and C showing a 100-kb region that includes a histone locus cluster (chr6:25,972,600-26,072,600).

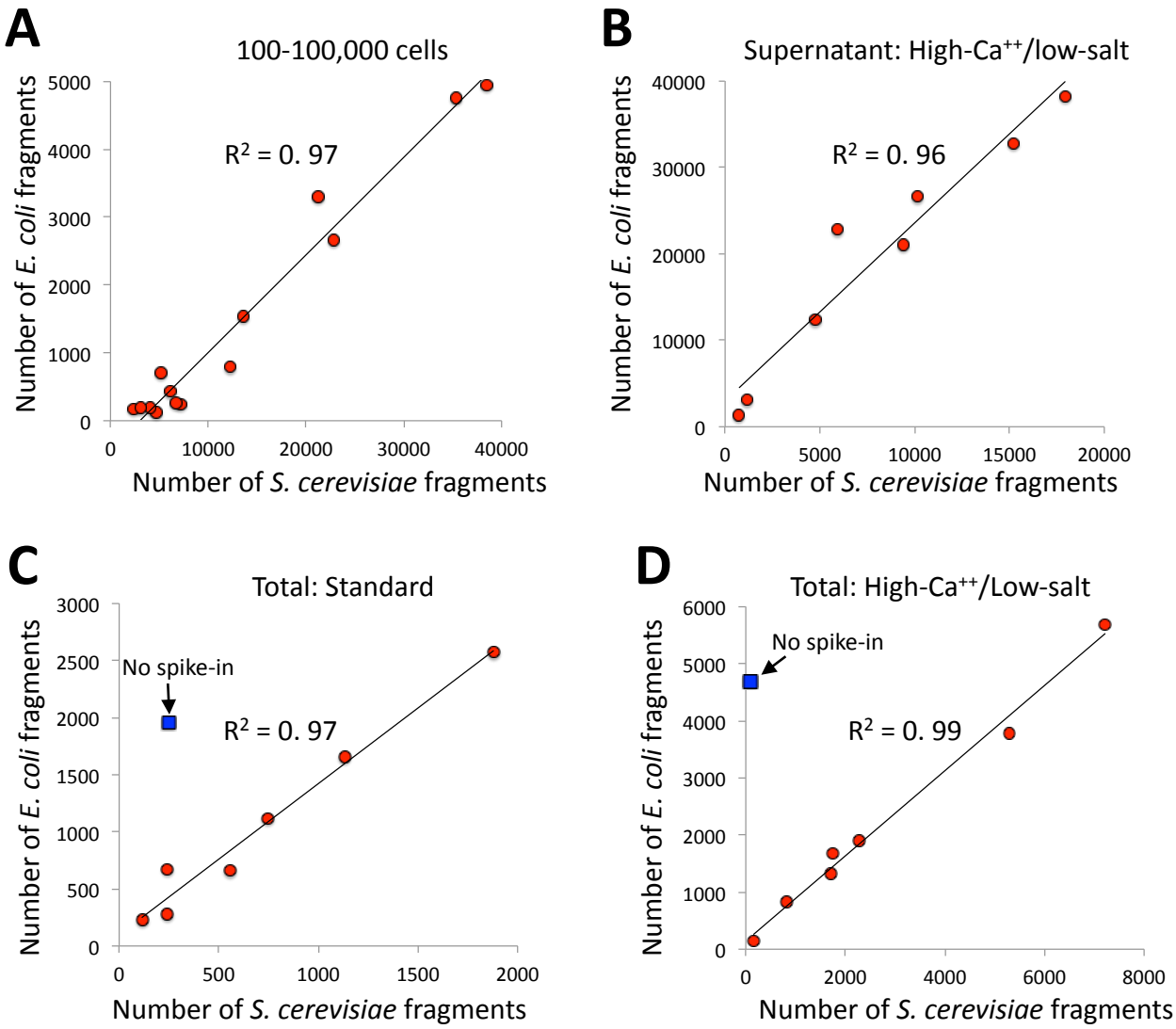

Figure 3. *E. coli* carry-over DNA of pA/MNase and pAG/MNase can substitute for spike-in calibration. A) Fragments from a CUT&RUN K562 cell experiment (GSE104550 20170426) using antibodies against H3K27me3 (100-8,000 cells) and CTCF (1,000-100,000 cells) were mapped to the repeat-masked genome of *S. cerevisae* and the full genome *E. coli*. Standard digestion was followed by supernatant release and extraction. **B**) Same as A using antibodies against multiple epitopes of varying abundances, high-calcium/low-salt digestion and supernatant release and extraction. **C**) Same as B except using standard digestion conditions and total DNA extraction. The *S.* cerevisiae spike-in DNA was left out for one sample (blue square). **D**) Same as C except using high-calcium/low-salt digestion and total DNA extraction.

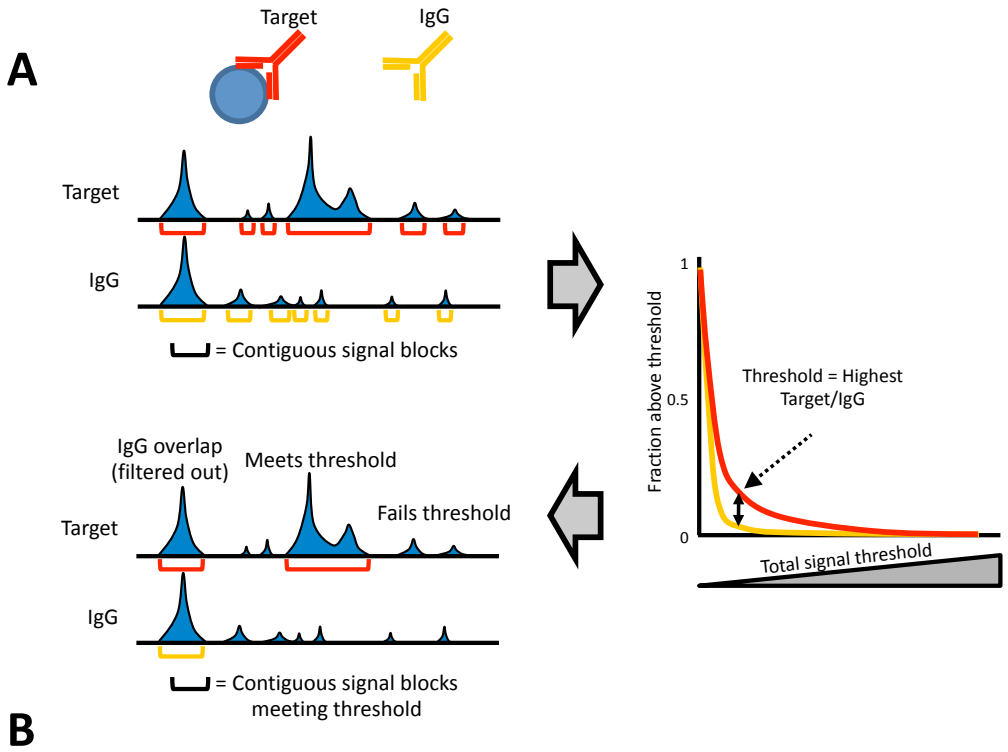

B

# of Peaks

SEACR (AUC only)	Sox2	FoxA2
hESC	17050	2
Endoderm	1	6215

# of Peaks

MACS2	Sox2	FoxA2
hESC	10728	858
Endoderm	695	7386

SEACR (union)	Sox2	FoxA2
hESC	19690	4
Endoderm	4	7327

HOMER	Sox2	FoxA2
hESC	7095	67
Endoderm	87	6493

Figure 4. SEACR enforces peak calling specificity across a range of read depths. A) Schematic of SEACR methodology. Contiguous signal blocks (top) are identified and plotted by the percentage of blocks exceeding a total signal threshold (right), and an optimal threshold is empirically identified and used for filtering (bottom). **B)** Peaks were called from Sox2 or FoxA2 experiments carried out in either hESCs or Endoderm cells using SEACR in AUC only or Union mode; MACS2; or HOMER.

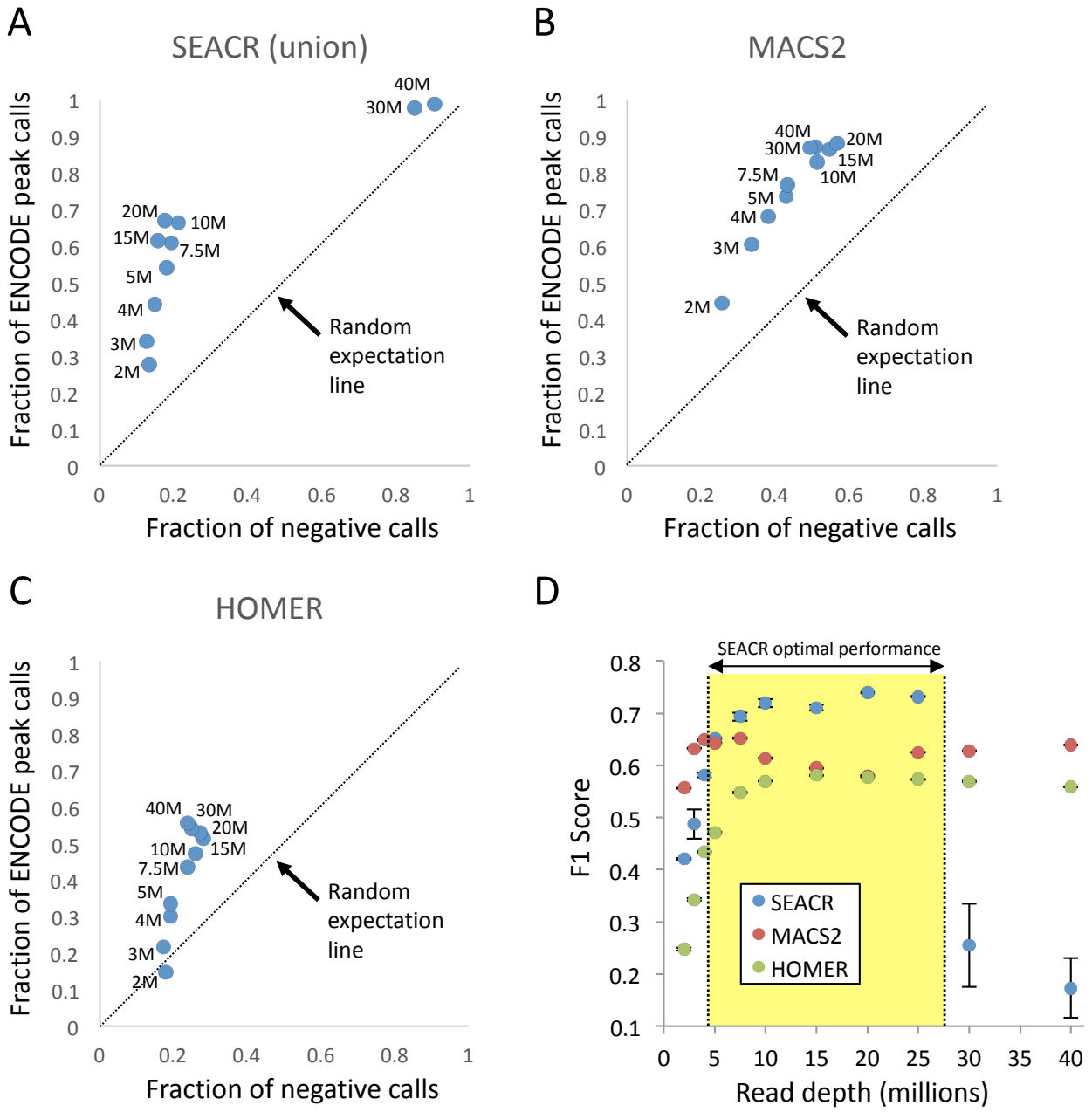

Figure 5. SEACR peak-calling provides an improved specificity/sensitivity trade-off. Fraction of ENCODE peaks called from subsampled H3K4me2 CUT&RUN data using SEACR Union mode (**A**), MACS2 (**B**), or HOMER (**C**). Subsampling level is indicated next to each point. **D)** F1 score for each point on the plots in A-C; read depths at which SEACR performance is superior are indicated by yellow shaded region.

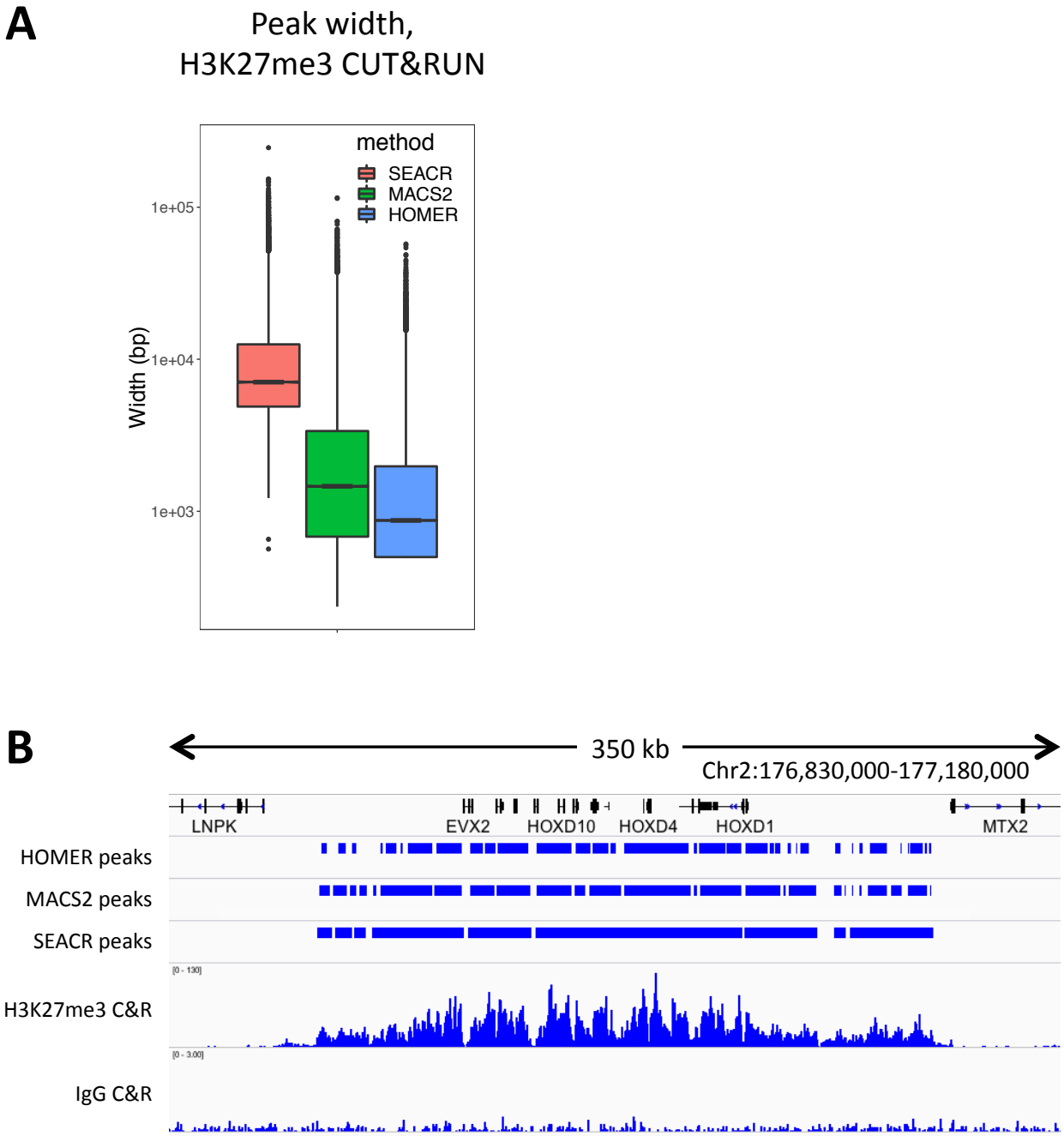

Figure 6. SEACR identifies coherent broad domains. A) CUT&RUN domains identified by SEACR are broader than those found by MACS2 or HOMER. **B**) A representative region of a H3K27me3 profile is shown. SEACR domains are relatively coherent compared with HOMER and MACS2 domains, which are fragmented into mixtures of wide and narrow segments.

A

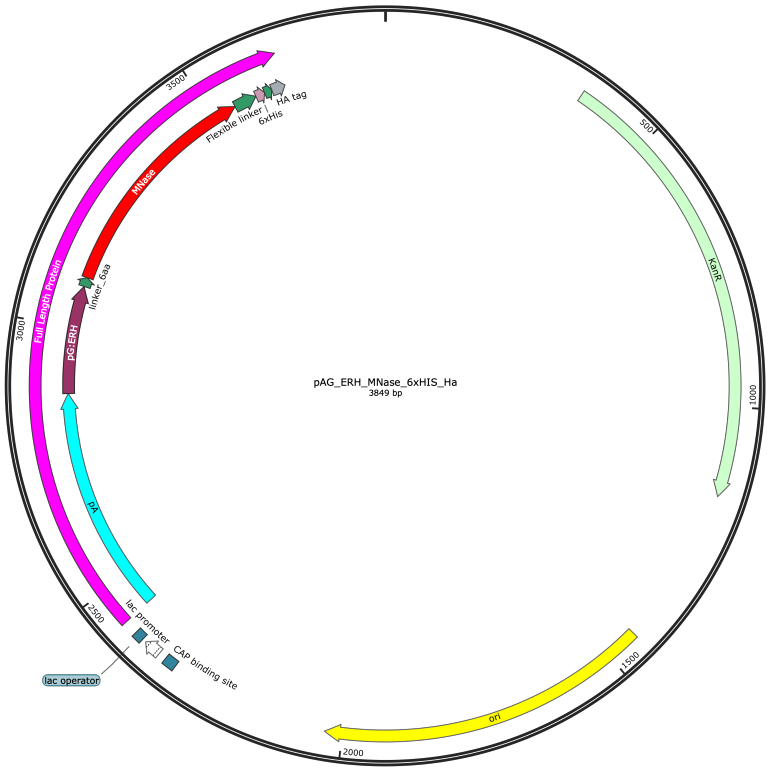

B

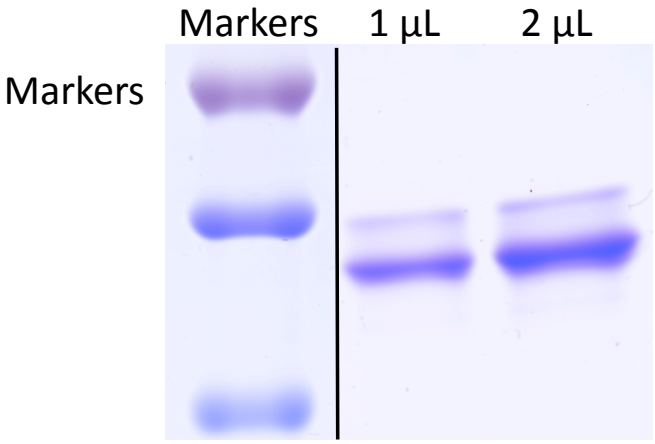

Figure 1 – figure supplement 1. An improved fusion protein for CUT&RUN. A) Plasmid map of pAG-ERH-MNase-6xHIS-HA. **B**) Coomassie-stained gel of fusion protein eluted from nickel-agarose.

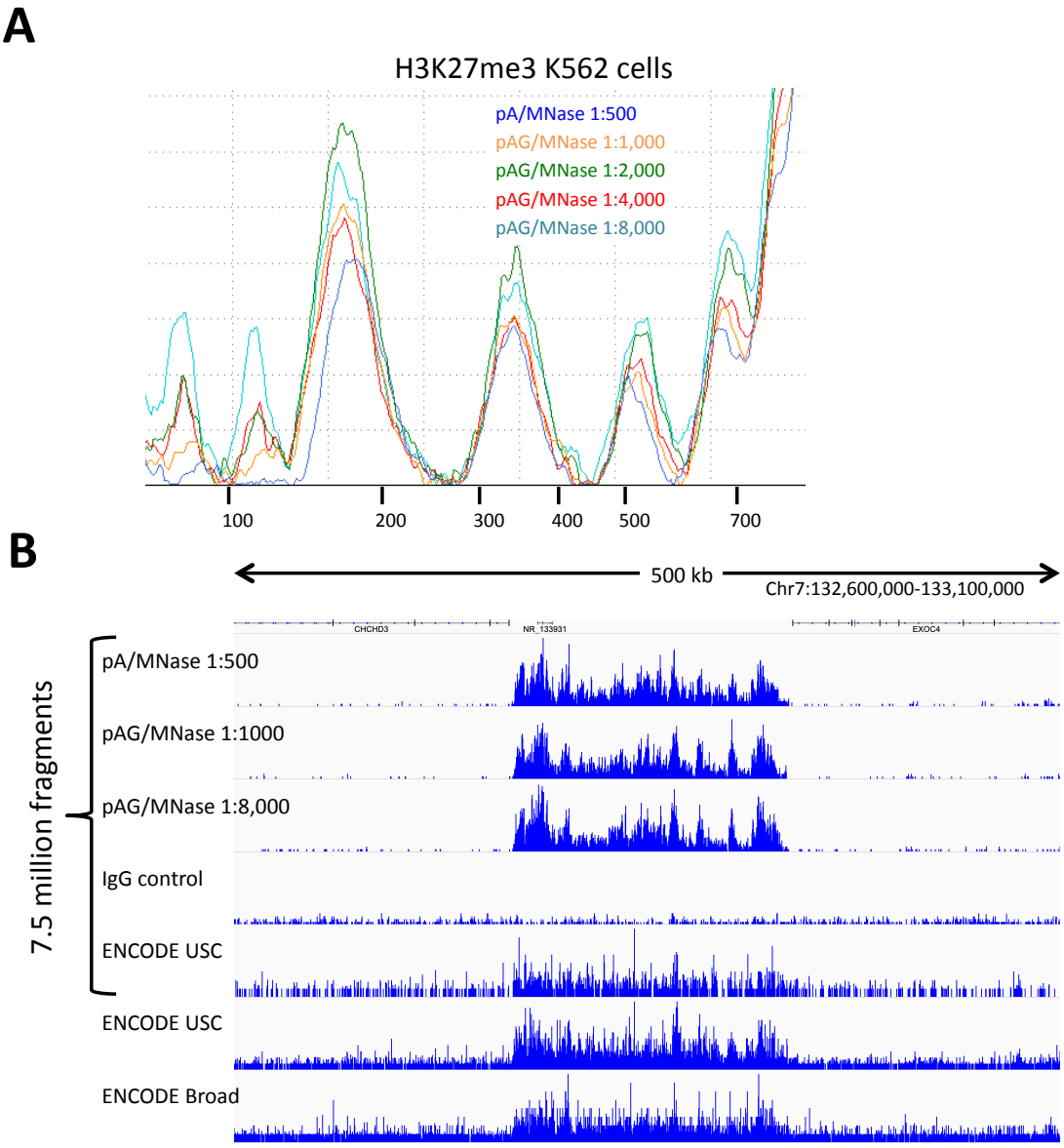

Figure 1 – figure supplement 2. pAG/MNase titration. A) K562 cells were incubated with an antibody to H3K27me3 (CST #9733 Rabbit monoclonal), washed twice with 1 ml Dig-wash. The sample was split into aliquots for incubation with pA/MNase at the recommended concentration and a serial dilution of pAG/MNase, followed by 3 1 ml washes. After 30 min using the standard protocol, llmit digestions are seen at all dilutions for this abundant epitope, indicating that the amount of fusion protein used in this experiment was in excess. **B**) Representative tracks from these samples show consistently low CUT&RUN backgrounds with excess pAG/MNase, which indicates that washes are sufficient to minimize non-specific background cleavages. ENCODE ChIP-seq tracks are shown for comparison, where USC used CST #9733, and Broad Institute used Millipore 07-449.

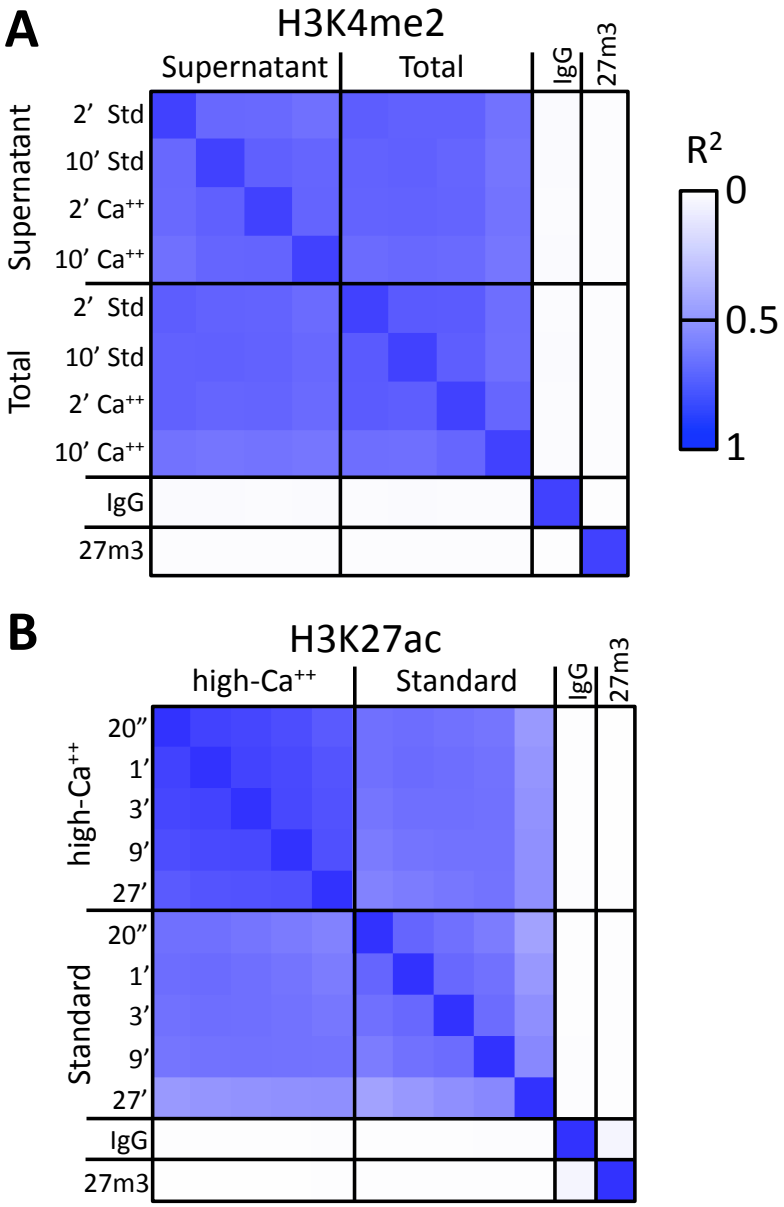

Figure 2 – figure supplement 1. CUT&RUN consistency with high-Ca++/low salt digestion and total DNA extraction. A) H3K4me2 CUT&RUN time points with digestions using either the standard protocol or the high-calcium/low-salt protocol with either supernatant or total DNA extraction. To construct the correlation matrix, all 8 H3K4me3 datasets were pooled and MACS2 was used to call peaks, which yielded 64,156 peaks. Peak positions were scored for each dataset and correlations (R^2 displayed with Java TreeView v.1.16r2, contrast = 1.25) were calculated between peak vectors. IgG and H3K27me3 (me3) negative controls were similarly scored. **B**) H3K27ac CUT&RUN time-course experiments were performed with an Abcam 4729 rabbit polyclonal antibody, following either the standard protocol or the low-salt/high-calcium (High-Ca^{++}) protocol. All 10 H3K27ac datasets were pooled and MACS2 called 54,431 peaks. Higher correlations between the High-Ca^{++} than the Std time points indicates improved uniformity of digestion despite the ~100-fold range of digestion times.

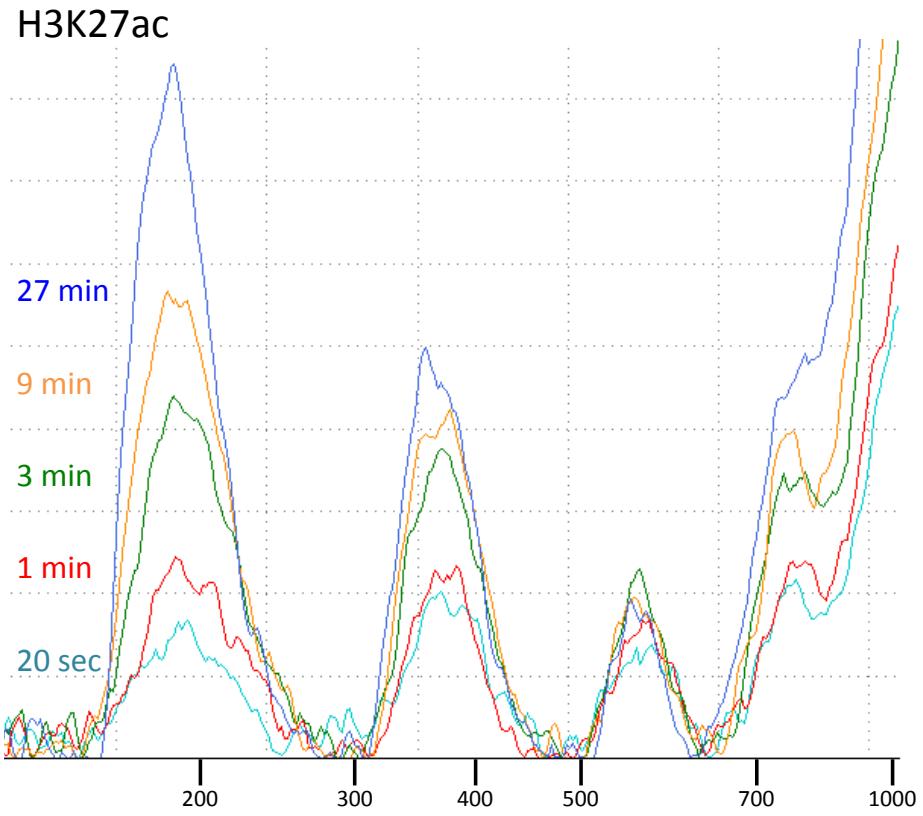

Figure 2 – figure supplement 2. Tapestation analyses of an H3K27ac digestion time-course series. CUT&RUN with the low-salt/high-calcium protocol results in fragment release within 20 seconds at 0 °C.

H3K27me3	Ab first	BSA	Human	Yeast	E. coli	Corr (Sc:Ec)
pA lo-hi			5913983	743	3455	0.92
pA lo-hi		+	7748003	858	4988	
pA lo-hi	+		5202278	2288	16110	
pA lo-hi	+	+	5178086	1804	18759	
pA std			6013347	595	2462	0.99
pA std		+	6005080	859	2295	
pA std	+		4104736	2624	21236	
pA std	+	+	3972820	2328	19245	
pAG lo-hi			6999802	789	404	0.94
pAG lo-hi		+	6374939	642	467	
pAG lo-hi	+		4140407	1565	1291	
pAG lo-hi	+	+	4058693	2382	5289	
pAG std			7514127	308	567	0.90
pAG std		+	5935592	355	125	
pAG std	+		4594153	1271	555	
pAG std	+	+	5379610	2509	1353	

Figure 3 – table supplement 1. Carry-over *E. coli* DNA correlates closely with the heterologous spike-in for both fusion proteins and both low-salt/high-calcium and standard digestion conditions. CUT&RUN was performed for H3K27me3 in parallel for pA/MNase Batch #6 (pA), pAG/MNase (pAG) using both low-salt/high-calcium (lo-hi) and standard (std) CUT&RUN digestion conditions. Each sample started with ~700,000 cells and 10 µL of bead slurry. Also varied in this experiment was addition of antibody followed by bead addition (Ab first) and addition of 0.1% BSA in the antibody buffer (BSA). Adding antibody first led to increased recovery of both yeast and E. coli DNA relative to human DNA, indicative of loss of cells prior to addition of fusion protein, possibly caused by loss of digitonin solubilization of membrane sugars.

A # of Bases Covered by Peaks

SEACR (AUC only)	Sox2	FoxA2
hESC	23405082	58704
Endoderm	68870	8366029

SEACR (union)	Sox2	FoxA2
hESC	25050747	81199
Endoderm	81311	9088596

MACS2	Sox2	FoxA2
hESC	4608040	591963
Endoderm	463996	2770715

HOMER	Sox2	FoxA2
hESC	1058250	4050
Endoderm	7050	967950

B % of Reads in Peaks

SEACR (AUC only)	Sox2	FoxA2
hESC	4.618	0.257
Endoderm	0.468	2.655

SEACR (union)	Sox2	FoxA2
hESC	4.962	0.911
Endoderm	0.935	2.882

MACS2	Sox2	FoxA2
hESC	7.386	4.198
Endoderm	3.456	5.857

HOMER	Sox2	FoxA2
hESC	1.434	0.005
Endoderm	0.007	1.487

Figure 4 – figure supplement 1. Peak calling metrics for SEACR. A-B) Table denoting the number of bases overlapped (A) or the percentage of reads in peaks (B) called by SEACR AUC only mode (top row), SEACR Union mode (second row), MACS2 (third row), or HOMER (fourth row). Factor and cell type from which data are derived are indicated in columns and rows, respectively.